Hindawi
Shock and Vibration
Volume 2020, Article ID 3518037, 12 pages
https://doi.org/10.1155/2020/3518037

Research Article

Study on Dynamic Characteristics of the Disc Spring System in Vibration Screen

Jiacheng Zhou, Chuzhe Zhang, Ziqiu Wang, and Kuanmin Mao

School of Mechanical Science & Engineering, Huazhong University of Science and Technology, Wuhan 430074, China

Correspondence should be addressed to Kuanmin Mao; kmmao4645@sina.com

Received 29 July 2019; Revised 1 December 2019; Accepted 6 January 2020; Published 10 February 2020

Academic Editor: Dario Di Maio

To avoid too large exciting force in traditional linear vibrating screen and unstable working state in resonance screen, the disc spring system is applied in the linear vibration screen. The model of the disc spring system in vibration screen is established by simulation and experiment. The characteristics of modal and amplitude of the disc spring system in vibration screen are studied. We found that the disc spring system vibrates in vertical direction at the third-order natural frequency, which is consistent with the direction of the vibration screen when screening particles. Moreover, the third-order natural frequencies in simulation and experiment are basically consistent. Furthermore, the maximum amplitude of the disc spring system appears at 960 r/min (16 Hz), which is in accord with the third-order natural frequency. Meanwhile, the amplitude increases proportionally with the increase of exciting force, while the amplification factors are the same under three different exciting forces. This indicates that the disc spring system has excellent linearity. The results of research provide guidance for design and application of elastic components on the vibration screen.

1. Introduction

The vibration of the large-scale machinery has always been a concern of engineers [1–3]. Vibration in heavy machinery often has a great impact on the performance and working accuracy of mechanical equipment [4]. At present, scholars have done many researches on vibration damping reduction and isolation of large-scale mechanical equipment. There are a variety of shock absorbers invented [5–7]. In order to reduce vibration, many researchers have studied the properties of spring [8]. In addition, structural optimization of mechanical equipment is also a common method of vibration reduction [9, 10]. However, the vibration in large-scale machinery is not always harmless; the vibration is needed in some machinery and equipment such as vibration screen [11].

Vibration screen is a type of mechanical equipment that completes the screening process and improves the screening efficiency according to the principle of vibration. So far, the vibration screen is extensively used in construction, mineral processing, metallurgy, petrochemical, grain, and other industrial fields [12, 13].

The linear vibrating screen is widely used in industry because of its simple structure and reliable operation. The helical spring is mainly adopted in traditional linear vibrating screen [14]. However, the low stiffness of helical spring leads to the lower natural frequency of traditional linear vibrating screen. Moreover, the natural frequency of the linear vibrating screen is very low and it is difficult to reach the working frequency [15]. As a result, the exciting force can not be reduced by using the principle of resonance. The exciting force required to obtain the working amplitude is too large [16, 17]. Therefore, the main components of vibration screen endure long time high strength loading, which results in fatigue failure of screen box and bearing [15–20].

Besides linear vibration screen, resonance screen is another kind of vibration screen, which is often used. The traditional resonance screen can reduce the exciting force by using the principle of resonance [21]. Nevertheless, the structure of traditional resonance screen is complex, and the nonlinear spring is usually used [22]. As a result, the natural frequency of the vibration screen is not a fixed value, which results in the unstable working state of the screen [23].

To avoid large exciting force in traditional linear vibrating screen and unstable working state in resonance screen, a new vibration screen, which has stable working state and small the exciting force, is needed.

The main reason for the different mechanical properties of the two vibration screens is that the springs they adopt are different. Spring is mechanical vibrator in vibration screen [24]. It is of great influence on the performance of vibration screen with different types of spring in vibration screen. Disc spring is a washer spring with a truncated conical section made of metal sheet or forged blank [25]. Compared with helical spring and nonlinear spring, disc spring has the characteristics of large load bearing capacity, stable working state, long service life, and high stiffness. Replacing helical spring with disc spring, the whole stiffness of linear screen can be improved, and the natural frequency of linear screen can be increased. Thus, the exciting force can be reduced by using the principle of resonance in linear screen with the disc spring. Therefore, it is necessary to study the dynamics characteristic of the disc spring system.

In this work, the disc spring system is applied in linear vibration screen. The model of the disc spring system in vibration screen is established both by simulation and experiment. The modal, amplitude, and amplification factors of the disc spring system in vibration screen are studied. The results show that the mechanical properties of the disc spring system have excellent linearity.

The natural frequency and mode shapes are obtained by simulation and experiment of modal test. Moreover, the amplitudes of the disc spring system under different rotational speeds are also investigated. Furthermore, the amplitudes experiment of the disc spring system under three different exciting forces are carried out. Comparing amplitudes and amplification factors under three different exciting forces, the linearity of the disc spring system is discussed.

2. Method and Methodology

2.1. Mechanical Model Description. Disc spring system is the main vibration component of vibrating screen. Figure 1(a) shows the experiment model of the disc spring system. According to the experiment model, the structural sketch is built in Figure 1(b).

As shown in Figure 1(b), the disc spring system is fixed on the workbench by bolt connection. The disc spring assembly is divided into two parts, one of which is located in the braced frame and the other is under the braced frame. The disc spring assembly is mounted on a shaft with a diameter of 120 mm. The upper part of the disc spring assembly is fixed and pretightened by the large-diameter screw nut. The mass block serves as load, which is located on the braced frame. The eccentric mass and the electric motor are connected to the system through the connecting plate.

2.2. Mechanic Analysis. According to the mechanical model and D'Alembert principle [26], the vibration equation of the vibration system is shown in formula (1). Referring to Figure 1(b), the force equations of disc spring system along X and Y directions are obtained in formula (1).

$$\begin{cases} Y:\ (-m\ddot{y}) + \left(-C_y\dot{y}\right) + \left(-k_y y\right) + \left[-m_0\ddot{y} + F_y(t)\right] = 0, \\ X:\ (-m\ddot{x}) + \left(-C_x\dot{x}\right) + \left(-k_x x\right) + \left[-m_0\ddot{x} + F_x(t)\right] = 0. \end{cases} \tag{1}$$

The masses of the experiment model and eccentric block are shown as m and m_0, respectively. The damping of the X and Y directions is shown as C_x and C_y, respectively. k_y and k_x represent the stiffness of the X and Y directions, respectively.

Inertial forces $F_x(t)$ and $F_y(t)$ of eccentric mass relative to rotary axis are shown in formula (2).

$$\begin{cases} F_x(t) = m_0\omega^2 r * \sin(\omega t), \\ F_y(t) = m_0\omega^2 r * \cos(\omega t). \end{cases} \tag{2}$$

Because the damping force and elastic force of liner vibrating screen are far less than the inertia force and exciting force of the screen, their influence on the motion of the screen is neglected in the approximate calculation [27].

The vibration equations of disc spring system along X and Y directions and rocking vibration equation around the centroid are obtained in formula (3).

$$\begin{cases} (m+m_0)\ddot{y} + C_y\dot{y} + k_y y = m_0\omega^2 r * \sin(\omega t), \\ (m+m_0)\ddot{x} + C_x\dot{x} + k_x x = m_0\omega^2 r * \cos(\omega t), \\ (J+J_0)\ddot{\varphi} = m_0\omega^2 r * \left[l_{y0}\cos(\omega t) - l_{x0}\sin(\omega t)\right] + T. \end{cases} \tag{3}$$

T represents the motor torque. However, comparing the loading torque produced by the eccentric mass, the motor torque is very small [27]. Therefore, the motor torque will be omitted in the following calculation.

J and J_0 are moment of inertia of the vibration system model and eccentric block to centroid of system. l_{x0} and l_{y0} are the distance of eccentric block rotating axis to system centroid along X and Y directions. $\ddot{\varphi}$ is angular acceleration of rocking vibration. Special solutions of differential formula (3) are shown in formula (4).

$$\begin{cases} y_0 = \lambda_{yA} * \cos(\omega t) + \lambda_{yB} * \sin(\omega t), \\ x_0 = \lambda_{xA} * \cos(\omega t) + \lambda_{xB} * \sin(\omega t), \\ \varphi = \lambda_{\Phi x} * \sin(\omega t) + \lambda_{\Phi y} * \cos(\omega t). \end{cases} \tag{4}$$

λ_y, λ_x, $\lambda_{\Phi x}$, and $\lambda_{\Phi y}$ are the amplitude and angle producing by exciting force and torque in Y and X directions.

Formula (4) is differentiated twice and brought into formula (3) to obtain

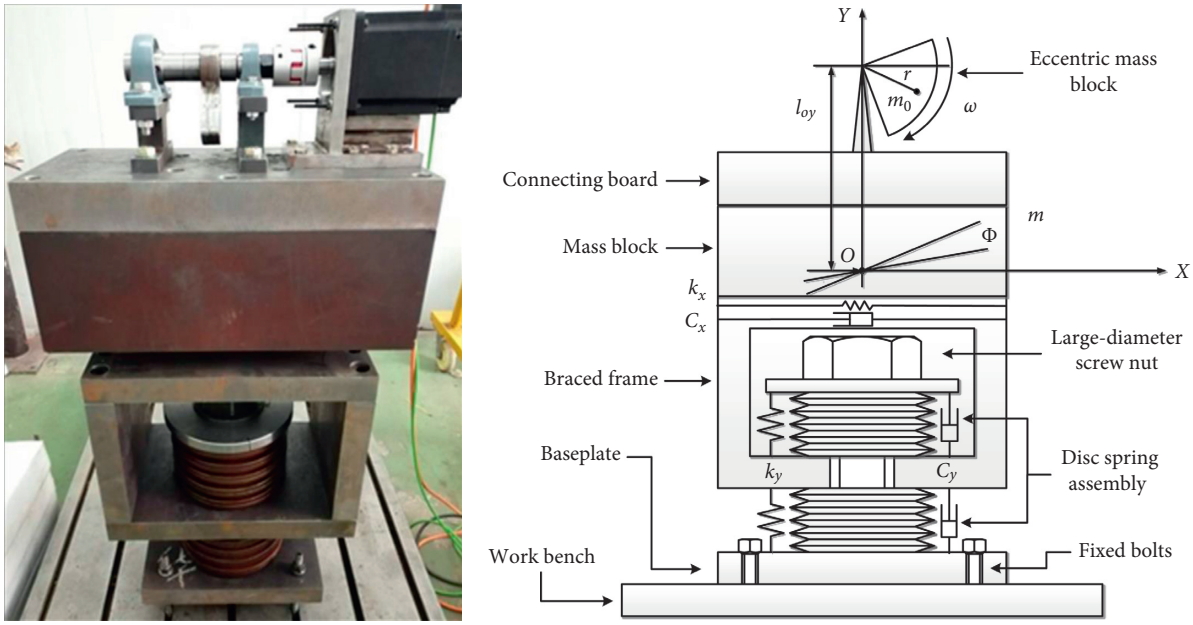

(a) (b)

Figure 1: Disc spring vibration system: (a) experiment model and (b) structural sketch.

$$\begin{cases} \lambda_{yA} = \dfrac{m_0\omega^3 r C_y}{\left[k_y - (m+m_0)\omega^2\right]^2 - \left(\omega C_y\right)^2}, \\ \lambda_{yB} = \dfrac{\left[k_y - (m+m_0)\omega^2\right] m_0\omega^2 r}{\left[k_y - (m+m_0)\omega^2\right]^2 - \left(\omega C_y\right)^2}, \\ \lambda_{xA} = \dfrac{\left[k_x - (m+m_0)\omega^2\right] m_0\omega^2 r}{\left[k_x - (m+m_0)\omega^2\right]^2 - \left(\omega C_x\right)^2}, \\ \lambda_{xB} = \dfrac{m_0\omega^3 r C_x}{\left[k_x - (m+m_0)\omega^2\right]^2 - \left(\omega C_x\right)^2}, \\ \lambda_{\Phi x} = \dfrac{m_0 r l_0 x}{J + J_0}, \\ \lambda_{\Phi y} = -\dfrac{m_0 r l_0 y}{J + J_0}. \end{cases} \tag{5}$$

The equation of motion for any point on the vibration system model is shown as follows:

$$\begin{cases} y_e = y_0 - \varphi l_{ex} = \left(\lambda_{yB} - \lambda_{\varphi x} l_{ex}\right) * \sin(\omega t) + \left(\lambda_{yA} - \lambda_{\varphi y} l_{ex}\right) * \cos(\omega t), \\ x_e = x_0 + \varphi l_{ey} = \left(\lambda_{yB} + \lambda_{\varphi x} l_{ey}\right) * \sin(\omega t) + \left(\lambda_{xA} + \lambda_{\varphi y} l_{ey}\right) * \cos(\omega t). \end{cases} \tag{6}$$

l_{ex} and l_{ey} are the distance of any point e to centroid of the vibration system along X and Y directions.

Using the above formulas, the modal parameters and amplitudes of the disc spring system can be calculated.

3. Simulation and Experimental Procedure

The specific procedure of the simulation and experiment of the disc spring system is shown in Figure 2.

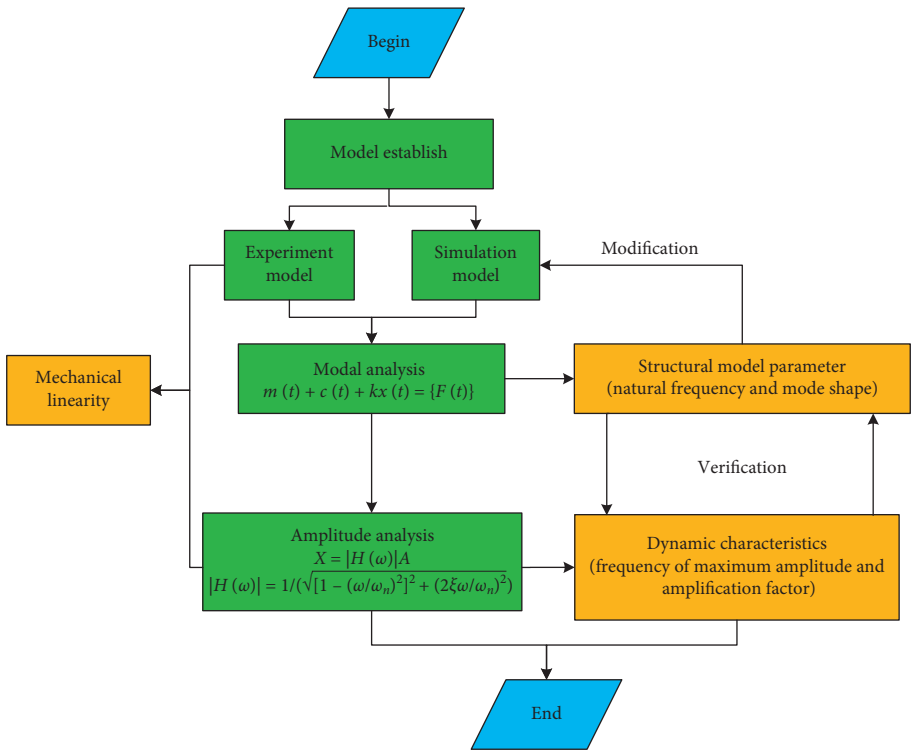

Figure 2: Flow chart for the proposed method.

3.1. Modal Simulation and Experiment. Modal testing is the technique that has been widely used in structural engineering for determining structural modal parameters, as natural frequencies, mode shapes, etc. [28, 29]. Frequencies and mode shapes represent the dynamic characteristics of structures and therefore are of fundamental importance for structural dynamics [30].

3.1.1. Natural Frequency of Disc Spring System. According to the theories of the free vibration without damping, the natural frequency f_n [31] of the disc spring system is shown in formula (7). ω_n stands for the natural angular frequency of the system and k refers to the stiffness of the disc spring system.

$$f_n = \frac{\omega_n}{2\pi} = \frac{1}{2\pi}\sqrt{\frac{k}{m}}. \tag{7}$$

By stiffness test, the stiffness of the disc spring assembly is 5675000 N/m on vertical direction. The mass of the whole disc spring system is around 620 kg. Through the frequency calculation, the natural frequency f_n of the disc spring system is calculated to be 15.23447 Hz. Considering the existence of the damping in the system [32], the actual natural frequency on vertical direction is slightly higher than the frequency of calculation.

3.1.2. Simulation of Modal Test

(1) Finite Element Model. To make sure the feasibility of the experiment, it is necessary to simulate with modal analysis using finite element analysis software.

The meshed finite element model is shown in Figure 3. The Solid185 [20] is adopted in element type, and the material parameters of finite element model are shown in Table 1.

According to the experimental conditions, the corresponding boundary conditions are applied to the model. There is a linear contact between the two disc springs. The surface-to-surface contact is adopted to other components. The upper and lower surfaces of the two sets of disc springs are set as full constraints. After preprocessor of the model, the Block Lanczos algorithm [33] is adopted in modal calculation.

3.1.3. Experiment of the Modal. The experiment is carried out after the simulation of the modal analysis. The method of impact testing is used to test the modal frequency and the mode shape of vibration system. The specific experimental equipment and scenarios are shown in Figure 4(a).

The vertical impacting excitation is generated by a heavy hammer on the upper surface of the vibration system. The four acceleration sensors are pasted on the geometric model nodes to receive acceleration signals. The Siemens data acquisition instrument (LMS SCADAS Mobile SCM05) is used to monitor and collect the time domain signal of the system [34]. By receiving and processing the signals of impact testing by modal analysis module, the actual natural frequency and mode shapes are obtained.

3.2. Amplitude Simulation and Experiment. In order to study the change of amplitude at resonance frequency, the amplitude simulation and experiment are carried out. In practical working condition, the working frequency of

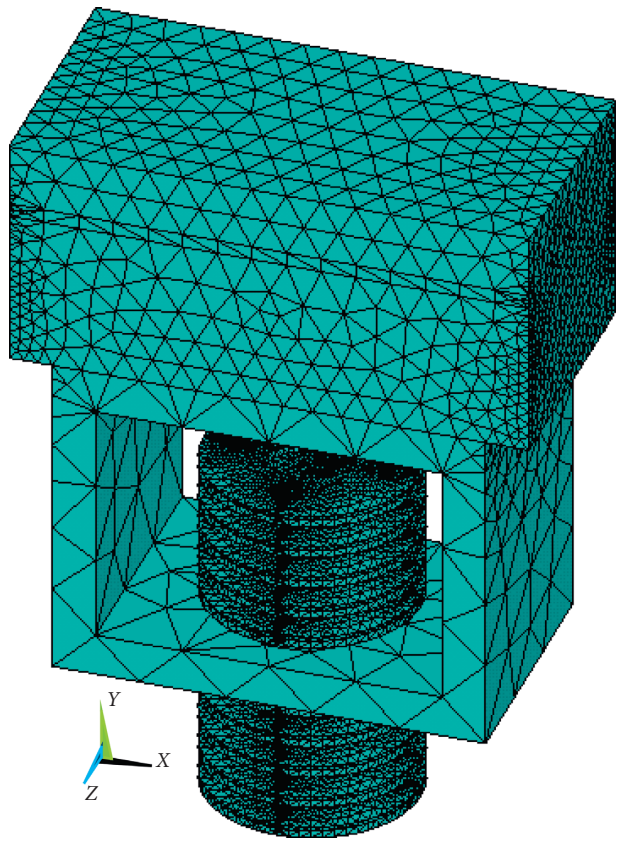

Figure 3: Simulation model of the disc spring system.

Table 1: Material parameters of finite element model.

Material	Density (kg/m^3)	Elastic modulus (GPa)	Poisson ratio
Mass block (gray cast iron)	7350	120	0.27
Braced frame (steel)	7900	210	0.25
Disc spring (spring steel)	7810	196.5	0.28

vibration screen can be adjusted by changing the speed of the driving motor. And the motor speed can be increased by 60 r/min (the working frequency is increased by 1 Hz) [35]. Therefore, working frequency of the disc spring system would be adjusted by changing the speed of the driving motor in experiment.

3.2.1. Simulation of Amplitude. The disc spring system model is established in modal analysis. The transient analysis module in finite element software is used to simulate the working process of vibration system [36]. By replacing exciting force produced by eccentric block, the dynamic force in the form of sine wave is exerted on the four corners of upper surface in vibration system.

The equation of dynamic force is shown as follows:

$$F = F_0 * \sin\left(f * \frac{\pi}{30} * \{\text{Time}\}\right). \quad (8)$$

F and F_0 are the dynamic force and centrifugal force produced by eccentric block at specified speed, respectively. f denotes the working frequency in the vibration system. And {Time} is time of duration in transient analysis. By changing the value of the working frequency f, the dynamic force under different working frequency is produced. According to actual working condition, the value of f varies from 13 Hz to 28 Hz. The full algorithm [37] is adopted in the transient analysis. The damping coefficient of disc spring system is set to be 0.1 [38]. The finite element (FE) model of the disc spring system is the same with modal analysis.

3.2.2. Experiment of Amplitude. The specific equipment and scenarios of amplitude experiment are shown in Figure 4(b). The rotation of eccentric block is driven by the motor; thus the dynamic force is produced. There are two laser displacement sensors. One laser displacement sensor is used to measure the real time surface amplitude of the vibration system. The other laser displacement sensor is used to monitor the real time surface amplitude of the workbench. The value of amplitude is collected by signal acquisition module in LMS. The actual amplitude of the disc spring vibration system is the difference between the amplitude of the upper surface and workbench.

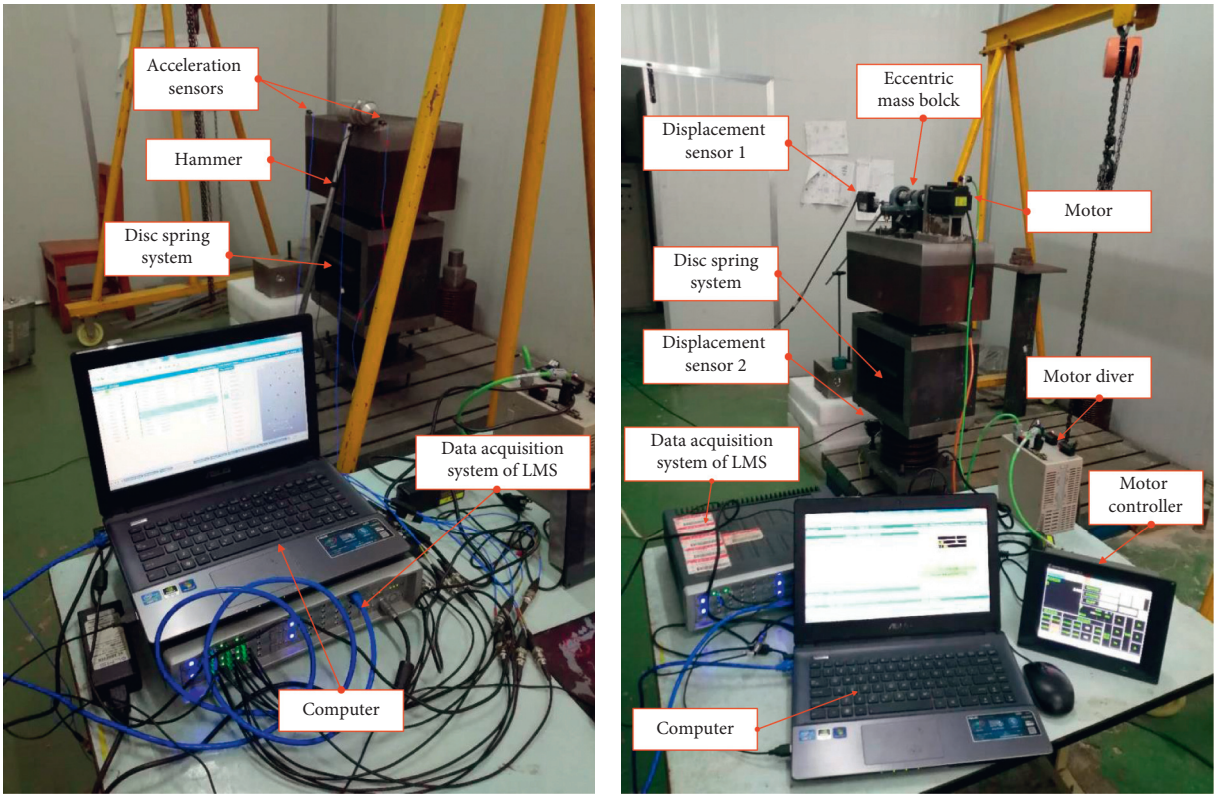

(a) (b)

Figure 4: Specific experimental equipment and scenarios: (a) modal test and (b) amplitude test.

4. Results and Discussion

4.1. Results of the Modal Simulation and Experiment

4.1.1. Simulation of the Modal Analysis. Figure 5 shows the mode shapes of the disc spring system in different natural frequencies. Figures 5(a)–5(d) correspond to the first, second, third, and fourth mode shapes of disc spring system, respectively. By observing the mode shapes under different orders, it can be seen that the model swings forward and backward along the Y direction at the first-order natural frequency (11.4374 Hz) in Figure 5(a), and the model swings left and right along the X direction at the second-order natural frequency (12.0005 Hz) in Figure 5(b). Then the model moves up and down along the Z direction at the third-order natural frequency (18.08 Hz) in Figure 5(c). At the fourth-order mode shape, the irregular distortion of the model occurs at the fourth-order natural frequency (79.5225 Hz) in Figure 5(d). Among the previous fourth mode shapes, the disc spring assembly has obvious deformation along the vertical direction in the third mode shape, which is consistent with the direction of the vibration screen when screening particles.

4.1.2. Experiment of the Modal Analysis. The primary three steps mode shapes of the system in experiment are shown in Figure 6. In order to facilitate the actual modal measurement, vibration signals of several key points on disc spring system are collected to represent the mode shape of the disc spring system. Four-point signals are collected on the circular surface of the disc spring to represent the mode shape of the circular surface of the disc spring. This kind of simplification does not affect the results of modal measurement.

The white wireframe in Figure 6 represents the model of the system itself, and the colored wireframe represents the mode shapes of the system at different natural frequencies. From Figure 6, it can be seen that the model vibrates along the Y, X, and Z directions in the previous third mode shapes, respectively, which is in good agreement with the simulation mode shapes in Figure 5.

To quantitatively compare the previous third-order natural frequencies of the disc spring system in simulation and experiment, the natural frequencies of experiments and simulations are shown in Table 2. It can be seen from Table 2 that the first three natural frequencies of experiment and simulation are basically consistent.

We can see that the mode shape and natural frequency of the disc spring system in simulation and experiment agree well with each other. Furthermore, the disc spring system vibrates in vertical direction at the third-order natural frequency, which is consistent with the direction of the vibration screen when screening particles.

4.2. Results of the Amplitude Simulation and Experiment

4.2.1. Simulation of the Amplitude. Figure 7 shows the amplitude of the disc spring system under four different

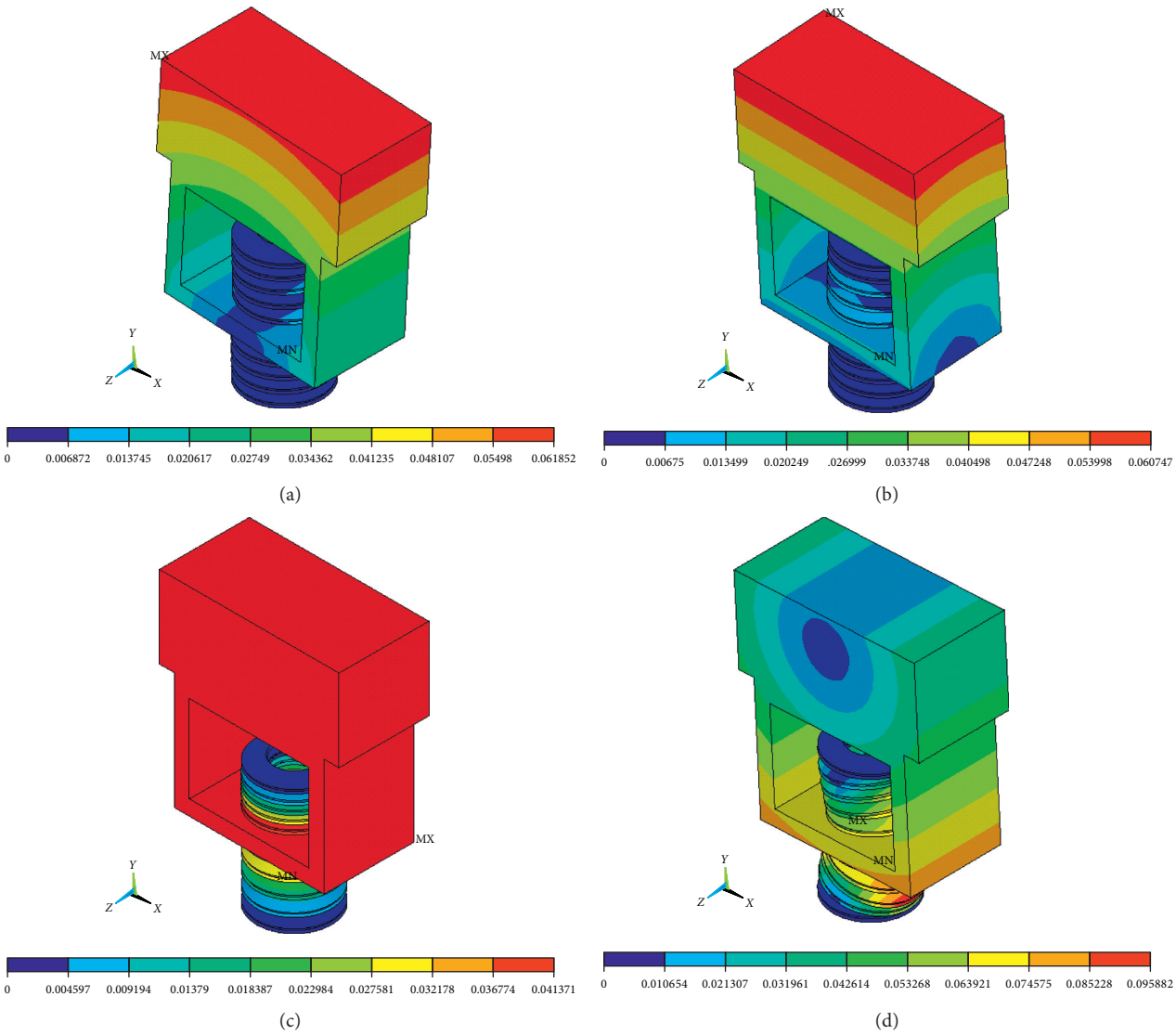

Figure 5: Previous four mode shapes and natural frequencies in simulation.

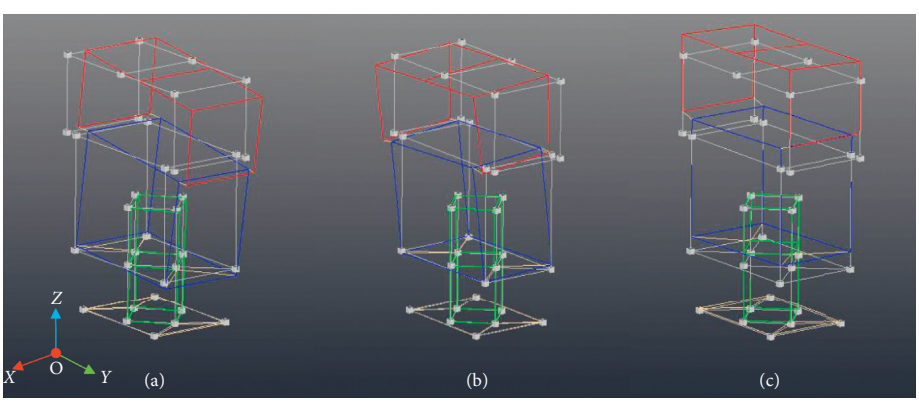

Figure 6: Previous three steps mode shapes of the disc spring system in experiment.

rotational speeds (frequencies) in simulation. The wave of amplitude in steady state is intercepted during the stable compelled vibration. And the time interval is 1 second. It can be seen that the amplitude of the disc spring system at 840 r/min (14 Hz) is 1.37 mm in Figure 7(a). As the rotational speed is increased to 1020 r/min (17 Hz), the amplitude of the disc spring system is 2.46 mm in Figure 7(b). The amplitude of the disc spring system is 1.63 mm and 0.95 mm at

Table 2: Natural frequencies of experiments and simulations.

Modal order	Natural frequencies (Hz)	
	Simulation	Experiment
1	11.437	11.002
2	12.000	11.473
3	18.080	16.470

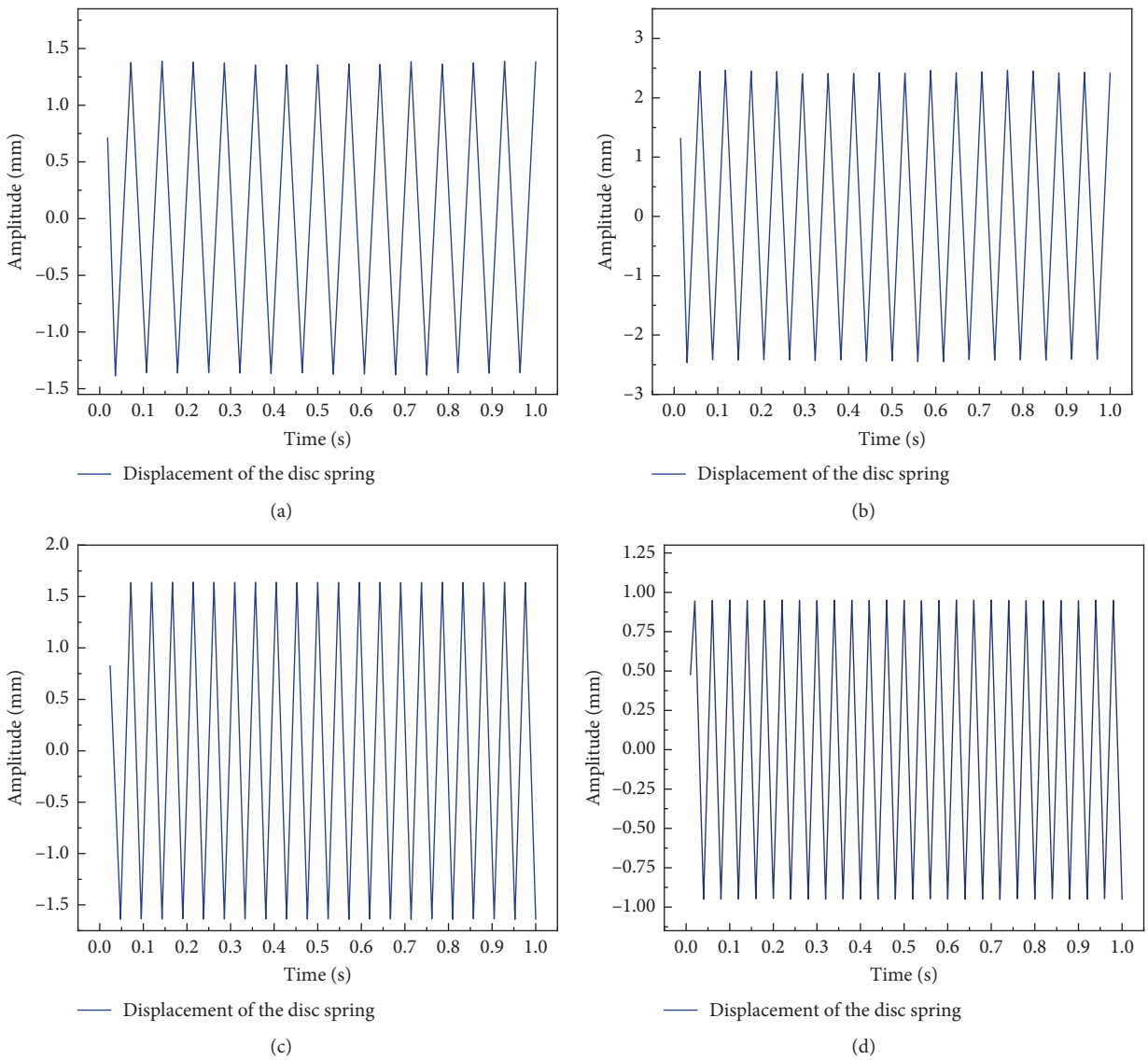

Figure 7: Simulation of the amplitude of the disc spring system under four different rotational speeds: (a) 840 r/min, (b) 1020 r/min, (c) 1260 r/min, and (d) 1500 r/min.

the rotational speed of 1260 r/min (21 Hz) and 1500 r/min (25 Hz) in Figures 7(c) and 7(d), respectively.

4.2.2. Experiment of the Amplitude. The corresponding experimental amplitudes in Figure 7 are shown in Figure 8. The wave of amplitude in steady state is intercepted during the stable compelled vibration. And the time interval is 1 second. The black curves represent the measured amplitude of the disc spring vibration system. The red curves represent the measured amplitude values of the workbench. The actual amplitude of the disc spring vibration system is the difference between the value of the black curve and red curve.

It can be seen that the amplitude of the disc spring system at 840 r/min (14 Hz) is 1.21 mm in Figure 8(a). As the rotational speed is increased to 1020 r/min (17 Hz), the amplitude of the disc spring system is 2.63 mm in Figure 8(b). The amplitude of the disc spring system is

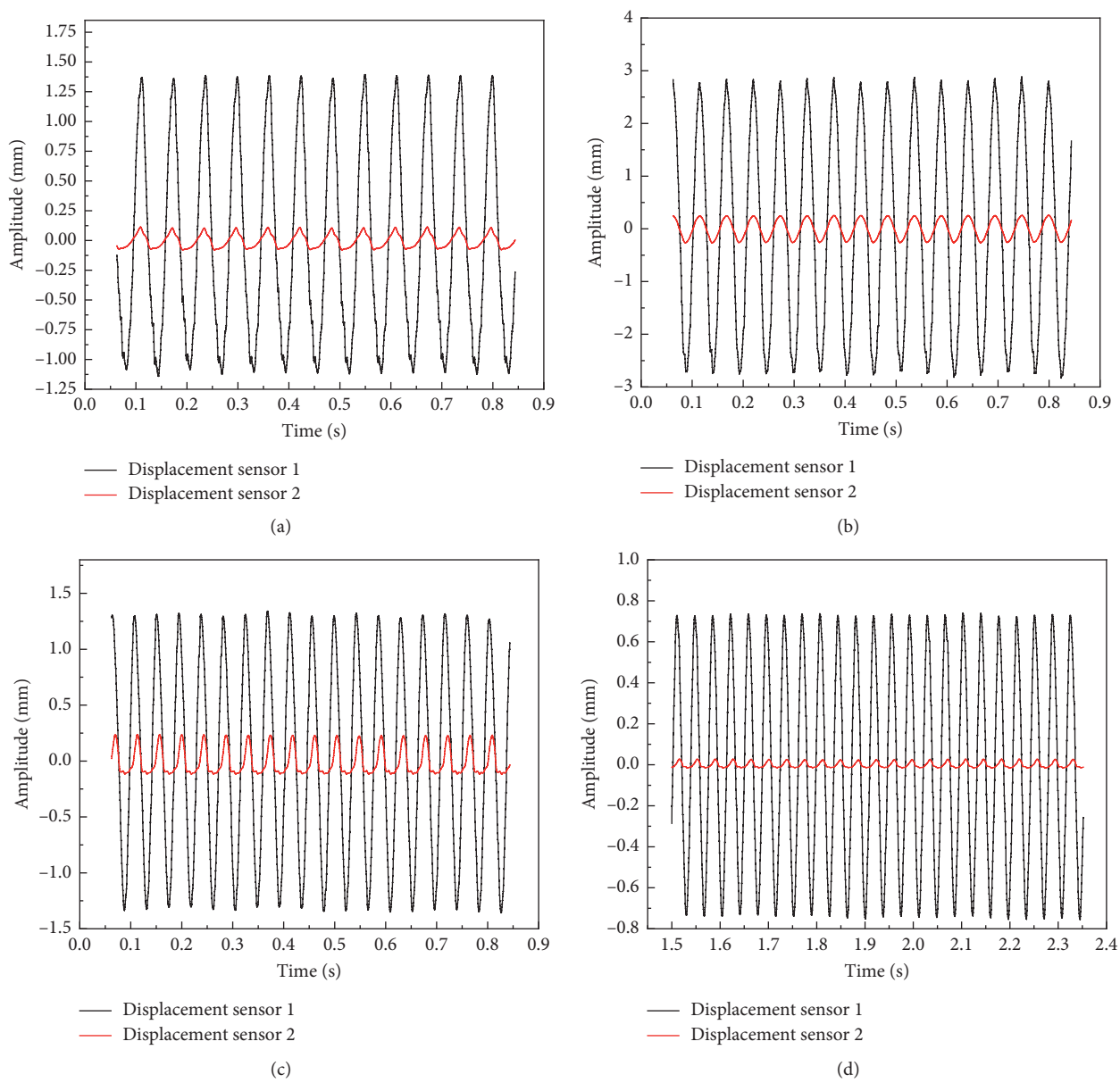

Figure 8: Experiment of amplitudes of experiment under four different rotational speeds: (a) 840 r/min, (b) 1020 r/min, (c) 1260 r/min, and (d) 1500 r/min.

0.98 mm and 0.68 mm at the rotational speed of 1260 r/min (21 Hz) and 1500 r/min (25 Hz) in Figures 8(c) and 8(d), respectively.

To quantitatively compare the amplitude in simulation and experiment, the amplitudes of the disc spring system under different rotational speeds are shown in Figure 9. The results show that the amplitude of the disc spring system in simulation increases as the rotational speed increases from 780 r/min (13 Hz) to 1080 r/min (18 Hz). When the rotational speed is further increased, the amplitude decreases as the rotational speed increases from 1080 r/min (18 Hz) to 1620 r/min (26 Hz). The maximum amplitude (3.89 mm) of the disc spring system appears at 1080 r/min (18 Hz), which is in accordance with the third-order natural frequency in simulation.

Moreover, the results show that the amplitude of the disc spring system increases as the rotational speed increases from 780 r/min (13 Hz) to 960 r/min (16 Hz). When the rotational speed is further increased, the amplitude decreases as the rotational speed increases from 960 r/min (16 Hz) to 1620 r/min (26 Hz). The maximum amplitude (3.3 mm) of the disc spring system appears at 960 r/min (16 Hz), which is in accordance with the third-order natural frequency in experiment.

Overall, the trend of simulation and experiment is consistent, and the numerical value is very close. The reason

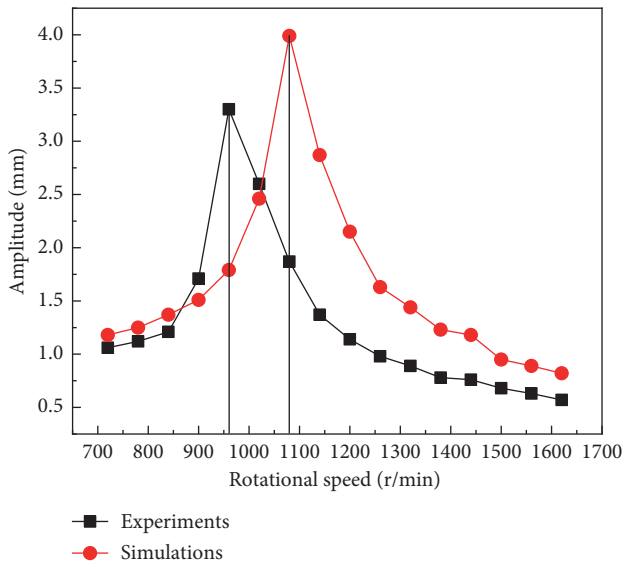

Figure 9: Amplitude comparison between experiment and simulation under different rotational speeds.

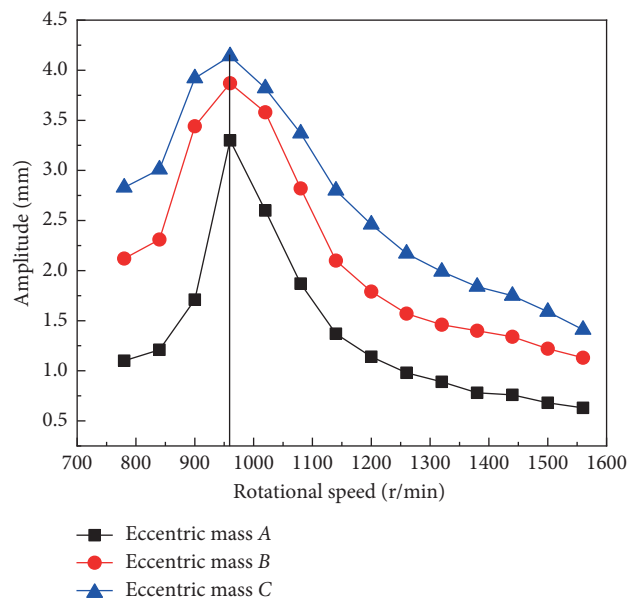

Figure 10: Amplitude of the disc spring system under three different eccentric masses.

for the error is that the damping coefficient in the simulation is smaller than that in experiment.

It should be noted that the amplitude is only 0.8 mm under the same magnitude of exciting force in the traditional vibration screen with the helical spring [39]. The amplitude of the disc spring system is around 4 times larger than the amplitude of traditional vibration screen. This means smaller exciting forces are required for the same amplitude the disc spring system in vibration screen, which saves energy and increases the fatigue life of vibration screen components.

In order to study the linearity between the amplitude of disc spring system and exciting force, the amplitudes of disc spring system under different exciting forces are shown in Figure 10. The different exciting forces are produced by the different rotating eccentric mass blocks. Three mass eccentric blocks A, B, and C are adopted. The mass of eccentric blocks A is 2.252 kg, and the eccentricity is 55.251 mm. The exciting forces produced by eccentric blocks B and C are 1.5 times and twice that of the exciting force produced by eccentric block A, respectively. It can be seen from Figure 10 that the three curves show a consistent trend of growth and decline. And the amplitude of the disc spring system increases as the exciting force. Meanwhile, the maximum amplitude of the disc spring system under three different exciting forces occurs at the same rotational speed of 960 r/min (16 Hz). In general, the disc spring system has a good mechanical linearity.

According to the theory of the force vibration with simple harmonic excitation, Amplitude X is proportional to the static displacement A [40].

$$X = |H(\omega)|A, \tag{9}$$

$$|\mathrm{H}(\omega)| = \frac{1}{\sqrt{\left[1-(\omega/\omega_n)^2\right]^2 + (2\xi\omega/\omega_n)^2}}. \tag{10}$$

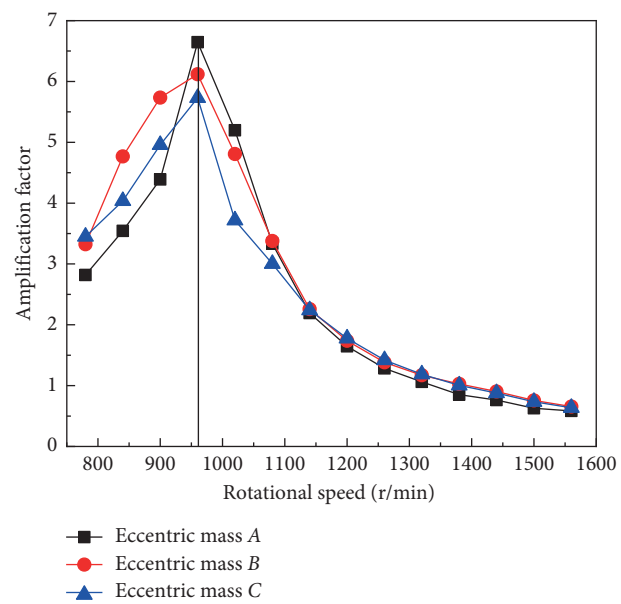

Figure 11: Amplification factor of three eccentric mass.

$|\mathrm{H}(\omega)|$ is the amplification factor of the disc spring vibration system. It stands for how much greater the amplitude X of dynamic vibration is than that of static displacement A. ξ and ω_n in formula (10) are the parameters of the system. ξ stands for the damping factor, and ω_n stands for the natural angular frequency of the system. By comparing the amplitude of the disc spring system under dynamic and static state, the amplification factor in each point can be calculated. The amplification factors under three different exciting forces are shown in Figure 11. It can be seen that the amplification factors increase as the rotational speed increases from 780 r/min to 960 r/min under three

different eccentric mass blocks. When the rotational speed is further increased from 960 r/min to 1620 r/min, the amplification factors decrease under three different eccentric mass blocks. The peak of the amplification factors appears at 16 Hz (960 r/min) under three different eccentric mass blocks. This is consistent with the law of vibration amplification [41]. The amplification coefficients under three different mass blocks are basically the same.

5. Conclusion

To avoid too large exciting force in traditional linear vibrating screen and unstable working state in resonance screen, the disc spring system is applied in the linear vibration screen. The dynamic characteristics of the disc spring system in vibration screen are studied. The model of the disc spring system in vibration screen is established by simulation and experiment. The characteristics of modal and amplitude of the disc spring system in vibration screen are studied. We found that the disc spring system vibrates in vertical direction at the third-order natural frequency, which is consistent with the direction of the vibration screen when screening particles. Meanwhile, the third-order natural frequency of the disc spring system in vibration screen is tested to be 18 Hz and 16 Hz in simulation and experiment, respectively. The mode shapes and natural frequency of simulation and experiment are basically, consistent.

Moreover, the amplitudes of the disc spring system under different rotational speeds are also investigated. The results show that the amplitude of the disc spring system increases as the rotational speed increases from 780 r/min (13 Hz) to 960 r/min (16 Hz). When the rotational speed is further increased, the amplitude decreases as the rotational speed increases from 960 r/min (16 Hz) to 1620 r/min (26 Hz). The maximum amplitude of the disc spring system appears at 960 r/min (16 Hz), which is in accordance with the third-order natural frequency. Besides rotational speed, the effects of the exciting forces on the amplitude of the disc spring system are investigated. The results show that the amplitude increases proportionally with the increase of exciting force. This indicates that the disc spring system has excellent linearity.

Furthermore, when comparing with the amplification factors in different rotational speeds, the results show that the amplification factor increases as the rotational speed increases from 780 r/min (13 Hz) to 960 r/min (16 Hz). When the rotational speed is further increased, the amplification factor decreases as the rotational speed increases from 960 r/min (16 Hz) to 1620 r/min (26 Hz). The maximum amplification factor appears at 960 r/min (16 Hz), which is in accordance with the third-order natural frequency. When comparing with the amplification factors in different exciting forces, the amplification factors remain basically the same.

The results of research provide guidance for design and application of elastic components on the vibration screen.

Data Availability

The data used to support the findings of this study are available from the corresponding author upon request.

Conflicts of Interest

The authors declare that they have no conflicts of interest.

Acknowledgments

The work of this paper was partially supported by the National High-Tech Research and Development Plan (863 Plan) (no. 2015AA043302). The authors acknowledge the help and advice by Dr. Lei Sheng in the strain and stress experiments.

References

[1] X. Zhang, Z. Wang, Y. Zhu, J. Xu, and B.-C. Wen, "Synchronization and stability of two pairs of reversed rotating exciters mounted on two different rigid frames," *IEEE Access*, vol. 7, pp. 115348–115367, 2019.

[2] X. Zhang, B. Wen, and C. Zhao, "Vibratory synchronization transmission of a cylindrical roller in a vibrating mechanical system excited by two exciters," *Mechanical Systems and Signal Processing*, vol. 96, pp. 88–103, 2017.

[3] X. Zhang, C. Li, Z. Wang, and S. Cui, "Synchronous stability of four homodromy vibrators in a vibrating system with double resonant types," *Shock and Vibration*, vol. 2018, Article ID 9641231, 20 pages, 2018.

[4] A. Jablonski and T. Barszcz, "Validation of vibration measurements for heavy duty machinery diagnostics," *Mechanical Systems and Signal Processing*, vol. 38, no. 1, pp. 248–263, 2013.

[5] W. Wu, X. Chen, and Y. Shan, "Analysis and experiment of a vibration isolator using a novel magnetic spring with negative stiffness," *Journal of Sound and Vibration*, vol. 333, no. 13, pp. 2958–2970, 2014.

[6] N. Zhou and K. Liu, "A tunable high-static-low-dynamic stiffness vibration isolator," *Journal of Sound and Vibration*, vol. 329, no. 9, pp. 1254–1273, 2010.

[7] Q. Li, Y. Zhu, D. Xu, J. Hu, W. Min, and L. Pang, "A negative stiffness vibration isolator using magnetic spring combined with rubber membrane," *Journal of Mechanical Science and Technology*, vol. 27, no. 3, pp. 813–824, 2013.

[8] G. A. Buxton, C. M. Care, and D. J. Cleaver, "A lattice spring model of heterogeneous materials with plasticity," *Modelling and Simulation in Materials Science and Engineering*, vol. 9, pp. 485–497, 2001.

[9] Y. Shen, L. Chen, X. Yang, D. Shi, and J. Yang, "Improved design of dynamic vibration absorber by using the inerter and its application in vehicle suspension," *Journal of Sound and Vibration*, vol. 361, pp. 148–158, 2016.

[10] J.-H. Zhu, W.-H. Zhang, and L. Xia, "Topology optimization in aircraft and aerospace structures design," *Archives of Computational Methods in Engineering*, vol. 23, no. 4, pp. 595–622, 2016.

[11] W. Raczka, M. Sibielak, J. Kowal, and J. Konieczny, "Application of an SMA spring for vibration screen control," *Journal of Low Frequency Noise, Vibration and Active Control*, vol. 32, no. 1-2, pp. 117–131, 2013.

[12] K. J. Dong, A. B. Yu, and I. Brake, "DEM simulation of particle flow on a multi-deck banana screen," *Minerals Engineering*, vol. 22, no. 11, pp. 910–920, 2009.

[13] Z. Li, X. Tong, B. Zhou, and X. Wang, "Modeling and parameter optimization for the design of vibrating screens," *Minerals Engineering*, vol. 83, pp. 149–155, 2015.

[14] M. L. Chandravanshi and A. K. Mukhopadhyay, "Analysis of variations in vibration behavior of vibratory feeder due to change in stiffness of helical springs using FEM and EMA methods," *Journal of the Brazilian Society of Mechanical Sciences and Engineering*, vol. 39, no. 9, pp. 3343–3362, 2017.

[15] Y.-M. Zhao, C.-S. Liu, X.-M. He, C.-Y. Zhang, Y.-B. Wang, and Z.-T. Ren, "Dynamic design theory and application of large vibrating screen," *Procedia Earth and Planetary Science*, vol. 1, no. 1, pp. 776–784, 2009.

[16] X. Du, "The kinematic analysis and simulation of the large-scale linear vibration screen," *Applied Mechanics and Materials*, vol. 215-216, pp. 726–729, 2012.

[17] C.-S. Liu, S.-M. Zhang, H.-P. Zhou et al., "Dynamic analysis and simulation of four-axis forced synchronizing banana vibrating screen of variable linear trajectory," *Journal of Central South University*, vol. 19, no. 6, pp. 1530–1536, 2012.

[18] Z. R. Zhang and Y. Y. Wang, "Deformation analysis of polyurethane screen deck in linear vibrating screen," *Advanced Materials Research*, vol. 221, pp. 240–246, 2011.

[19] W. E. Whiteman and M. S. Berman, "Fatigue failure results for multi-axial versus uniaxial stress screen vibration testing," *Shock and Vibration*, vol. 9, Article ID 109715, 10 pages, 2002.

[20] L.-P. Peng, C.-S. Liu, B.-C. Song, J.-D. Wu, and S. Wang, "Improvement for design of beam structures in large vibrating screen considering bending and random vibration," *Journal of Central South University*, vol. 22, no. 9, pp. 3380–3388, 2015.

[21] J. N. Eiras, J. Monzó, J. Payá, T. Kundu, and J. S. Popovics, "Non-classical nonlinear feature extraction from standard resonance vibration data for damage detection," *The Journal of the Acoustical Society of America*, vol. 135, no. 2, pp. EL82–EL87, 2014.

[22] S. J. Zhu, Y. F. Zheng, and Y. M. Fu, "Analysis of non-linear dynamics of a two-degree-of-freedom vibration system with non-linear damping and non-linear spring," *Journal of Sound and Vibration*, vol. 271, no. 1-2, pp. 15–24, 2004.

[23] L. I. Slepyan and V. I. Slepyan, "Coupled mode parametric resonance in a vibrating screen model," *Mechanical Systems and Signal Processing*, vol. 43, no. 1-2, pp. 295–304, 2014.

[24] L.-P. Peng, C.-S. Liu, J. Li, and H. Wang, "Static-deformation based fault diagnosis for damping spring of large vibrating screen," *Journal of Central South University*, vol. 21, no. 4, pp. 1313–1321, 2014.

[25] C. K. H. Dharan and J. A. Bauman, "Composite disc springs," *Composites Part A: Applied Science and Manufacturing*, vol. 38, no. 12, pp. 2511–2516, 2007.

[26] Y. Nakamura and M. Ghodoussi, "A computational scheme of closed link robot dynamics derived by D'Alembert principle," in *Proceedings of IEEE International Conference on Robotics & Automation*, April 1988.

[27] B. Wen and S. Liu, *Modern Vibration Screen Technology and Equipment Design*, Metallurgical Industry Press Co., Beijing, China, 3rd edition, 2013.

[28] J.-J. Wu, "Finite element modelling and experimental modal testing of a three-dimensional framework," *International Journal of Mechanical Sciences*, vol. 46, no. 8, pp. 1245–1266, 2004.

[29] E. Reynders, K. Maes, G. Lombaert, and G. De Roeck, "Uncertainty quantification in operational modal analysis with stochastic subspace identification: validation and applications," *Mechanical Systems and Signal Processing*, vol. 66-67, pp. 13–30, 2016.

[30] S. Lei, K. Mao, L. Li, W. Xiao, and B. Li, "Sensitivity analysis of modal assurance criteria of damped systems," *Journal of Vibration and Control*, vol. 23, no. 4, pp. 632–644, 2017.

[31] S. Kong, S. Zhou, Z. Nie, and K. Wang, "The size-dependent natural frequency of Bernoulli-Euler micro-beams," *International Journal of Engineering Science*, vol. 46, no. 5, pp. 427–437, 2008.

[32] H. Okamoto, D. Ito, K. Onomitsu et al., "Vibration amplification, damping, and self-oscillations in micromechanical resonators induced by optomechanical coupling through carrier excitation," *Physical Review Letters*, vol. 106, no. 3, pp. 1–4, 2011.

[33] L. Dahmani, A. Khennane, and S. Kaci, "Crack identification in reinforced concrete beams using ANSYS software," *Strength of Materials*, vol. 42, no. 2, pp. 232–240, 2010.

[34] K. Mao, M. Zhu, W. Xiao, and B. Li, "A method of using turning process excitation to determine dynamic cutting coefficients," *International Journal of Machine Tools and Manufacture*, vol. 87, pp. 49–60, 2014.

[35] M. Hagiwara, K. Nishimura, and H. Akagi, "A medium-voltage motor drive with a modular multilevel PWM inverter," *IEEE Transactions on Power Electronics*, vol. 25, no. 7, pp. 1786–1799, 2010.

[36] Y. F. Shu and Y. F. Zheng, "Transient dynamics analysis of the reachstacker speader based on ANSYS," *Advanced Materials Research*, vol. 1078, pp. 212–215, 2014.

[37] S.-K. Kim, J.-H. Jeon, C.-H. Cho, E.-S. Kim, and J.-B. Ahn, "Modeling and simulation of a grid-connected PV generation system for electromagnetic transient analysis," *Solar Energy*, vol. 83, no. 5, pp. 664–678, 2009.

[38] J. Gao, *Study on Disc Spring-High Damping Rubber Isolation Bearing*, Beijing University of Technology, Beijing, China, 2018.

[39] J. W. Phillips and G. A. Costello, "Large deflections of impacted helical springs," *The Journal of the Acoustical Society of America*, vol. 51, no. 3B, pp. 967–973, 1972.

[40] N. A. Ubaidillah, K. Hudha, and F. A. A. Kadir, "Modelling, characterisation and force tracking control of a magneto-rheological damper under harmonic excitation," *International Journal of Modelling, Identification and Control*, vol. 13, no. 1-2, pp. 9–21, 2011.

[41] E. Savin, "Dynamic amplification factor and response spectrum for the evaluation of vibrations of beams under successive moving loads," *Journal of Sound and Vibration*, vol. 248, no. 2, pp. 267–288, 2001.